KRATOS: KOLLISION RISK ASSESSMENT TOOL IN ORBITAL ELEMENT SPACES

Joshua T. Horwood, Navraj Singh, and Jeffrey M. Aristoff

Numerica Corporation, 5042 Technology Parkway, Suite 100, Fort Collins, CO 80528

Apoorva Bhopale

Air Force Research Laboratory, 3550 Aberdeen Avenue SE, Kirtland AFB, NM 87117

ABSTRACT

KRATOS provides an innovative approach to computing the probability of collision (PC) between resident space objects that reduces misdetection and false alarms rates and supports the mission's goal of performing conjunction assessment screening further out into the future. Although applicable to all regimes of space, KRATOS was designed to treat objects in the challenging non-linear and non-Gaussian regimes. KRATOS rivals the accuracy of Monte-Carlo methods but with little added computational cost relative to the traditional linearization (Foster) method. This paper provides an overview of the KRATOS algorithm and demonstrates its efficacy using real and simulated data. Scenarios are presented in which use of the Foster method would produce false alarms or misdetections, and hence would misinform the analyst. Use of KRATOS in these scenarios provides a reliable PC, as verified using Monte-Carlo simulation, and hence would better inform the analyst.

1. INTRODUCTION

Traditional methodologies for assessing collision risk between resident space objects (RSOs) can produce misdetections and false alarms. The resulting probabilities of collision (PCs) can be too high, implying a high false alarm rate and the need to perform costly and unnecessary evasive maneuvers, or too low, meaning that some potential collisions go undetected, which could have dire consequences. The desire to perform conjunction assessment (CA) screening further out into the future, up to one week for Low Earth Objects (LEOs), for example, adds to the challenge of providing reliable space situational awareness (SSA). Thus, what is needed are new methodologies that reduce these false alarm and misdetection rates, and hence better inform courses of action.

As the PC calculation is far too expensive to perform on all possible pairs of objects, one first employs techniques called conjunction filtering that aim to quickly rule out infeasible conjunctions at a computational cost less than that of a full PC calculation. After a filter or set of filters returns all feasible conjunction pairs, one then proceeds to quantify the collision risk by computing the PC on each remaining pair. Linearization techniques based on the Foster method [1] make several simplifying assumptions in the PC calculation including that of a realistic Gaussian covariance in position-velocity space of the two approaching objects at the time-of-closest approach (TCA). With the desire to do CA further out into the future and uncorrelated tracks (UCTs) generated from the new Space Fence that will inevitably possess large covariances, non-linear effects will become more pronounced, resulting in a breakdown of covariance realism and rendering the Gaussian assumption in Foster's method invalid. Methods that relax the Gaussian assumption will be needed in the future; some preliminary research on computing the PC using Gaussian mixtures models has been considered by DeMars, Cheng, and Jah [2] as part of the Adaptive Entropy Gaussian Information Synthesis (AEGIS) algorithm [3]. Alternatively, Monte-Carlo simulation can be used, but it is too computationally demanding to apply on all high risk events.

The Kollision Risk Assessment Tool in Orbital Element Spaces (KRATOS) provides a new approach to computing the PC between RSOs that supports the mission's goal of performing CA screening further out into the future. Although applicable to all regimes of space, KRATOS was designed to treat objects in the challenging non-linear and non-Gaussian regimes by relaxing the Gaussian assumptions present in the traditional Foster method. In such challenging regimes, KRATOS is able to efficiently compute the PC over much longer screening intervals than what is currently possible, by leveraging the Numerica's prior work in Gaussian mixture filters

and orbital element coordinate systems, including the newly-developed J_2 equinoctial orbital elements [4]. These innovative features of KRATOS permit a robust computation of the PC integral without having to represent a space object's uncertainty as a potentially inaccurate Gaussian distribution in Cartesian space, as is needed in Foster's method.

In this paper, we provide an overview of the KRATOS algorithm. Using both real and simulated Vector Covariance Message (VCM) data, we demonstrate scenarios in which the Foster method produces false alarms and misdetections, and hence would misinform the analyst. Use of KRATOS in these scenarios provides a reliable PC with accuracy that rivals more computationally expensive Monte-Carlo simulation, and hence would better inform the analyst. KRATOS is computationally viable, with runtimes that can be many orders of magnitude less than Monte-Carlo approaches. These runtime differences are especially pronounced in cases involving operational spacecraft when the PC is around the threshold value at which the decision to maneuver would be made, and when a large number of Monte-Carlo trials would be needed to achieve sufficient accuracy. The computational efficiency of KRATOS is due, in part, to only having to propagate a single Gaussian in J_2 element space to the nominal TCA rather than an entire Gaussian mixture in Cartesian space. Evidence of this high performance is presented in this paper, and comparisons to other Gaussian-mixture-based approaches are made.

2. METHODOLOGY

A widely-used methodology for assessing the risk of collision between two RSOs based on the PC uses a formulation due to Foster [1] from the early 1990s. Here, the PC is expressed as a two-dimensional integral on the plane orthogonal to the relative velocity vector at the TCA, called the encounter plane, over which the swept-out volume of the hard ball and the relative position Gaussian probability density function (PDF) are projected. Specifically,

$$P_c = \frac{1}{2\pi\sigma_y\sigma_z} \int_{-R}^{R} \int_{-\sqrt{R^2-y^2}}^{\sqrt{R^2-y^2}} \exp\left[-\frac{1}{2}\left(\frac{y-y_m}{\sigma_y}\right)^2 - \frac{1}{2}\left(\frac{z-z_m}{\sigma_z}\right)^2\right] \mathrm{d}z\,\mathrm{d}y, \tag{1}$$

where R is the combined radius of the two objects, the integration variables y and z are aligned with the minor and major axes of the (projected) relative position covariance ellipsoid, y_m and z_m are the respective components of the projected miss distance, and σ_y and σ_z are the respective standard deviations. Figure 1, adapted from Alfano [5], visualizes the conjunction scenario and the covariance sliced by the encounter plane.

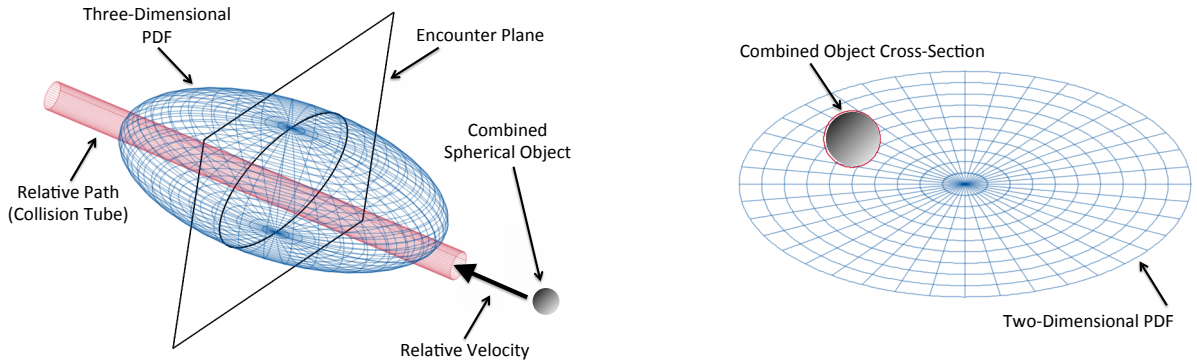

Figure 1. Visualization of the Conjunction Encounter Implied in the Foster Method (left) and the Covariance Sliced by the Encounter Plane (right). Figure Adapted from Alfano [5].

Foster's method builds in several assumptions on the physics and statistics of the conjuncting objects. Chief amongst these is the assumption that the encounter be short-term meaning that the relative motion can be approximated as rectilinear at the conjunction. Additionally, at the conjunction, the PDFs of the two objects are assumed Gaussian with respect to Cartesian position-velocity coordinates, the combined position covariance is constant, and the relative velocity uncertainty is zero. The formulation also assumes that the input states and covariances of the two objects defined at some epoch time (prior to the conjunction) are realistic. Ultimately,

it is the responsibility of the user to provide realistic data to serve as input to the Foster method (or any PC algorithm for that matter); further remarks on this requirement are made in Section 4.

While the rectilinear motion assumption at conjunction is valid for most pairs of objects in LEO, the Gaussian assumption can be violated over long screening times, or if one or both objects have large errors (i.e., large epoch covariances). The former assumption is significant since some of the current practices may hinder the goal of performing CA screening out to seven days in LEO. Regarding the latter assumption, as evidenced in prior work by Numerica and others on non-linear uncertainty propagation [6, 7], covariance realism can degrade in scenarios when insufficient data has been collected on a RSO, especially on newly-formed UCTs. For some LEO UCTs, this breakdown can come as early as a quarter of an orbital period. Thus, this previous research and mission objectives motivate the need to relax the traditional assumption of Gaussianity.

To address these challenges, KRATOS provides a more robust PC algorithm that relaxes some of the assumptions implicit in the current Foster method in order to achieve a more reliable collision risk assessment metric. Some of the key innovations in KRATOS include (i) treatment of *non-Gaussian PDFs* in order to improve robustness in non-linear regimes, better handle UCTs with large errors, and facilitate longer screening periods; (ii) use of *Gauss-Hermite quadrature (GHQ)*, also known as the unscented transform [8], to more faithfully propagate states and covariances to TCA, without loss of realism; (iii) performing said propagations *directly in orbital element space*, including the new J_2 *equinoctial orbital elements* [4], to prolong covariance realism even longer; and (iv) leveraging Numerica's prior work on *Gaussian mixtures* [6, 9, 10] to achieve improved accuracy in the PC computation with realistic runtimes.

In describing the KRATOS algorithm, we begin by establishing some notation and definitions. We consider two RSOs, labeled the 'primary' (index a) and 'secondary' (index b), with respective position-velocity state vectors $\boldsymbol{x}_a = (\boldsymbol{r}_a, \boldsymbol{v}_a)$ and $\boldsymbol{x}_b = (\boldsymbol{r}_b, \boldsymbol{r}_b)$, where $\boldsymbol{r}_i$, $i = a, b$, denotes the position component and $\boldsymbol{v}_i$ denotes the velocity. The dependence of the vectors on time is omitted unless stated otherwise. The relative motion state vector is denoted as $\boldsymbol{x} = (\boldsymbol{r}, \boldsymbol{v})$ and is centered at the primary such that

$$\boldsymbol{x} = \boldsymbol{x}_b - \boldsymbol{x}_a, \quad \boldsymbol{r} = \boldsymbol{r}_b - \boldsymbol{r}_a, \quad \boldsymbol{v} = \boldsymbol{v}_b - \boldsymbol{v}_a.$$

Given an epoch time t_0, a screening time of interest T, and a radius threshold $R > 0$, the two objects are said to collide if there exists a time $t \in [t_0, t_0 + T]$ such that $\|\boldsymbol{r}(t)\| \leq R$. The radius threshold is usually chosen as the sum of the hard-body radii of the two objects. It is assumed that the joint (12-dimensional) PDF $p_{a,b}(\boldsymbol{x}_a, \boldsymbol{x}_b, t)$ is known at any given time t within the screening period along with the marginal (6-dimensional) PDFs $p_a(\boldsymbol{x}_a, t)$ and $p_b(\boldsymbol{x}_b, t)$. Typically, these PDFs are provided at epoch (and are usually Gaussian) and, subject to a dynamical model, can be computed at a future time t using traditional techniques such as linearized propagation (for the Gaussian case), or other techniques such as the GHQ or Gaussian mixtures. We refer the reader to the Astrodynamics Innovations Committee (AIC) Covariance Realism Working Group report [11] for a detailed exposition on the many uncertainty propagation techniques that are presently in use or have been proposed for use in the space surveillance environment. Based on these definitions, the PC is

$$P_c = \int_V p_{a,b}(\boldsymbol{X}_0, t_0)\, \mathrm{d}\boldsymbol{X}_0, \tag{2}$$

where $\boldsymbol{X}_0 = (\boldsymbol{x}_a(t_0), \boldsymbol{x}_b(t_0))$ and $V \subseteq \mathbb{R}^{12}$ is the set of initial conditions for which a collision occurs on $[t_0, t_0 + T]$. The integral (2) facilitates the PC computation using a Monte-Carlo simulation.

To balance the high computational demand of the Monte-Carlo evaluation of the general PC integral (2) with the need to provide a more accurate PC that relaxes some of the assumptions in the classic Foster method, the formulation of the PC in KRATOS makes the following basic assumptions:

A1. *Only one crossing.* Each collision trajectory satisfies the condition $\|\boldsymbol{r}(t)\| = R$ with $\boldsymbol{v}(t) \cdot \boldsymbol{r}(t) \leq 0$ just once on the interval $(t_0, t_0 + T]$.

A2. *Trajectories must cross.* No collision trajectories satisfy $\|\boldsymbol{r}(t)\| = R$ for a finite time interval.

A3. *Independence.* The PDF for each object is independent. In other words, $p_{a,b}(\boldsymbol{x}_a, \boldsymbol{x}_b, t) = p_a(\boldsymbol{x}_a, t)\, p_b(\boldsymbol{x}_b, t)$ for all $t \in [t_0, t_0 + T]$.

By applying a hierarchy of assumptions, beginning with (A1)–(A3), Coppola [12] shows how the integral (2) simplifies and eventually reduces to the Foster method integral (1). Indeed, imposing Assumptions (A1)–(A2) on (2) leads to

$$P_c = -\int_{t_0}^{t_0+T} \int_{0}^{2\pi} \int_{-\pi/2}^{\pi/2} \int_{\boldsymbol{v}\cdot\boldsymbol{r}\le 0} p_\Delta(\boldsymbol{x}, t)\, \boldsymbol{v}\cdot\hat{\boldsymbol{r}}\, R^2 \cos\theta \,\mathrm{d}\boldsymbol{v}\,\mathrm{d}\theta\,\mathrm{d}\phi\,\mathrm{d}t. \tag{3}$$

In this equation, $\hat{\boldsymbol{r}}$ is the unit vector $\boldsymbol{r}/\|\boldsymbol{r}\|$, and

$$p_\Delta(\boldsymbol{x}, t) = \int_{-\infty}^{\infty} p_{a,b}(\boldsymbol{x}_a, \boldsymbol{x}_a + \boldsymbol{x}, t)\,\mathrm{d}\boldsymbol{x}_a = \int_{-\infty}^{\infty} p_a(\boldsymbol{x}_a, t)\, p_b(\boldsymbol{x}_a + \boldsymbol{x}, t)\,\mathrm{d}\boldsymbol{x}_a, \tag{4}$$

where the independence assumption (A3) has been invoked. We acknowledge that the PC integral (3) does not account for the instantaneous PC at t_0. Although it can be incorporated into the PC computation (see Coppola [12]), we omit its inclusion in this discussion since it is negligible for the scenarios presented in this paper.

KRATOS assumes that the relative motion PDF (4) can be approximated as a *Gaussian mixture*. Such a PDF has the form

$$p_\Delta(\boldsymbol{x}, t) = \sum_{k=1}^{N} w^{(k)}\, \mathcal{N}\big(\boldsymbol{x}; \boldsymbol{\mu}^{(k)}(t), \mathbf{P}^{(k)}(t)\big), \tag{5}$$

where $\mathcal{N}$ denotes the Gaussian distribution defined by

$$\mathcal{N}(\boldsymbol{x}; \boldsymbol{\mu}, \mathbf{P}) = \frac{1}{\sqrt{\det(2\pi\mathbf{P})}}\, \exp\left[-\frac{1}{2}(\boldsymbol{x}-\boldsymbol{\mu})^T \mathbf{P}^{-1} (\boldsymbol{x}-\boldsymbol{\mu})\right].$$

Further, the given weights $w^{(k)}$, $k = 1, \ldots, N$, are non-negative scalars which sum to unity, and $\boldsymbol{\mu}^{(k)}$ and $\mathbf{P}^{(k)}$ are the mean and covariance of the k-th Gaussian component (all defined at time t). Substituting the Gaussian mixture representation (5) into the PC integral (3) leads to

$$P_c = \sum_{k=1}^{N} w^{(k)} P_c^{(k)},$$

where

$$P_c^{(k)} = -\int_{t_0}^{t_0+T} \int_{0}^{2\pi} \int_{-\pi/2}^{\pi/2} \int_{\boldsymbol{v}\cdot\boldsymbol{r}\le 0} \mathcal{N}\big(\boldsymbol{x}; \boldsymbol{\mu}^{(k)}(t), \mathbf{P}^{(k)}(t)\big)\, \boldsymbol{v}\cdot\hat{\boldsymbol{r}}\, R^2 \cos\theta \,\mathrm{d}\boldsymbol{v}\,\mathrm{d}\theta\,\mathrm{d}\phi\,\mathrm{d}t. \tag{6}$$

In this formulation, the PC is a weighted sum of PC integrals, where each component (6) implicitly imposes Assumptions (A1)–(A3) in addition to the Gaussian assumption. To proceed, we define additional assumptions, following the presentation in Coppola [12].

A4. *Gaussian distribution.* The PDF $\mathcal{N}\big(\boldsymbol{x}; \boldsymbol{\mu}^{(k)}(t), \mathbf{P}^{(k)}(t)\big)$ remains Gaussian for all $t \in [t_0, t_0 + T]$.

A5. *No velocity uncertainty.* The PDF $\mathcal{N}\big(\boldsymbol{x}; \boldsymbol{\mu}^{(k)}(t), \mathbf{P}^{(k)}(t)\big)$ depends only on position and time.

A6. *Short encounter time.* The duration of the conjunction is sufficiently short so that the relative motion can be approximated as rectilinear and the relative position covariance is constant.

A7. *Time integrates out.* The integration interval $[t_0, t_0 + T]$ can be replaced by the interval $(-\infty, \infty)$, so long as Assumption (A6) is not violated.

While Assumptions (A4)–(A7) are not directly imposed to the PC integral (3), KRATOS imposes these assumptions on each of the component PC integrals (6), thereby reducing each of them to the Foster method integral (1). Such assumptions are well-justified, especially for short-term encounters in LEO, and if the Gaussian mixture (5) is an accurate representation of the actual relative motion PDF. Additional commentary on the relaxation of these assumptions is provided in Section 4.

The main inputs to the Gaussian mixture-based method for computing the PC in KRATOS are the following.

- Epoch time t_0 and a screening time T. These two inputs define the screening interval $[t_0, t_0 + T]$.
- Gaussian PDFs of the primary and secondary at epoch, represented by mean-covariance pairs in *equinoctial orbital elements (EqOE)*. The VCM format provides such input. If the epoch Gaussians are provided in another coordinate system (e.g., Cartesian position-velocity coordinates), then they can be converted to the required input using, for example, the GHQ algorithm (unscented transform) [10].
- Screening radius R. If the primary and secondary object sizes are known, then R is the sum of their hard-body radii, otherwise R is a user-defined parameter (e.g., 25 meters).
- Orbital propagator function that maps an orbital state $\boldsymbol{x}_0$ at time t_0 with respect to Cartesian inertial position-velocity coordinates to the state $\boldsymbol{x}(t)$ at some (past or future) time t, subject to a dynamical model. If using VCMs as input, the different force model parameters used in the propagation (e.g., gravity model, drag, solar radiation pressure) are encoded in this format.

At a high level, the main steps in the algorithm are as follows.

1. Estimate the nominal (mean) TCA and its standard deviation.
2. Propagate the states and covariances of the primary and secondary from epoch to the nominal TCA using GHQ with an orbital element coordinate system.
3. Transform the primary and secondary Gaussians in orbital element coordinates to corresponding Gaussian mixtures in Cartesian coordinates.
4. Represent the relative motion PDF as a Gaussian mixture.
5. Apply the Foster method on each Gaussian component.

A schematic illustrating this processing chain is depicted in Figure 2. It is beyond the scope of this paper to give full mathematical details on each of these steps. Instead, we conclude this section with a few closing remarks.

- In Step 1, the TCA is a random variable since it is a function of the input primary and secondary Gaussian states at epoch. We define the nominal TCA to be the mean of the TCA random variable. Along with the variance (or standard deviation) in the TCA, it can be computed using the GHQ or unscented transform.
- In Step 2, propagation "with an orbital element coordinate system" is *not* restricted to analytical or semi-analytical techniques such as SGP4. Individual GHQ nodes or "sigma points" can be propagated using any general- or special-perturbations-based method. For the latter, the nodes or sigma points are typically propagated in Cartesian space (since the force models are naturally provided in these coordinates), yet the final Gaussian (at the nominal TCA) is reconstructed and represented in element space.
- The output of Step 2 is the mean-covariance pairs of the primary and secondary with respect to EqOE coordinates defined at the nominal TCA. This step can use the J_2 equinoctial orbital elements (J_2EqOE) [4] in place of the traditional EqOE coordinates. The use of any non-singular system of six orbital elements, such as the equinoctial set, is well-suited to the problem of uncertainty propagation under the perturbed two-body problem, since they absorb the most dominant non-linear term in the equations of motion (i.e., the $1/r^2$ term). Hence, propagation is less non-linear in orbital elements, thereby more closely preserving Gaussian and linear approximations. One can ask if improvements are possible. Indeed, the J_2EqOE coordinates effectively absorb the J_2 perturbation and are non-singular for all non-inclined or circular orbits. Thus, use of the J_2EqOEs can significantly prolong covariance realism over the classical EqOEs.

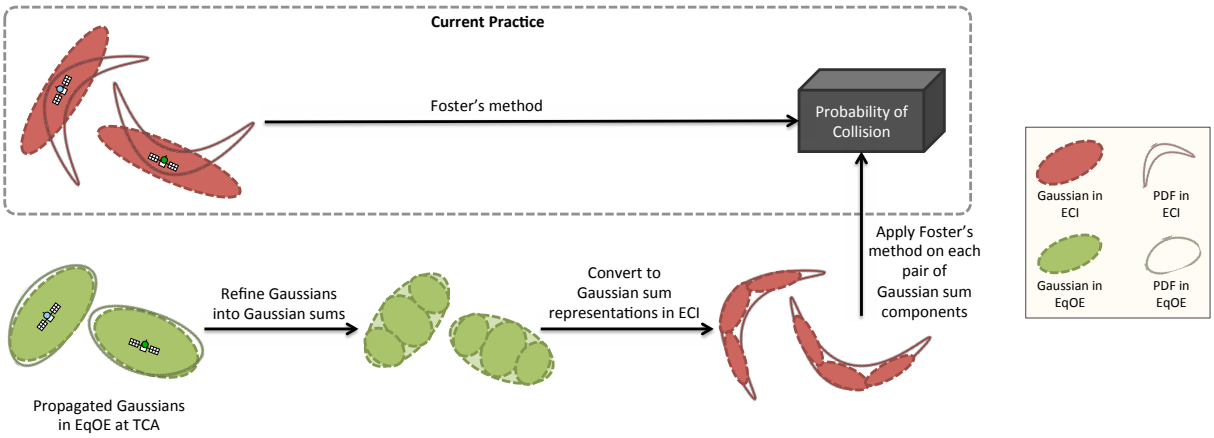

Figure 2. Schematic of the KRATOS Algorithm for Computing the PC

- DeMars, Cheng, and Jah [2] also propose using a Gaussian mixture representation of the primary and secondary in Cartesian coordinates at the nominal TCA, to facilitate the application of the Foster method. However, they obtain this representation by first refining the Gaussian PDF at the epoch time t_0 into a Gaussian mixture and then propagating each of the mixture components to the nominal TCA. The AEGIS algorithm [3] is used for this propagation. In contrast, KRATOS only requires the propagation of *a single Gaussian* PDF in element space (rather than a mixture of Gaussians), as described in Step 2. Although in Step 3 we still need to convert each mixture component to Cartesian space, this operation is significantly cheaper than having to propagate a mixture component under the non-linear dynamics [10]. The relative merits of these two approaches are studied in Section 3.

3. RESULTS AND DISCUSSION

Erroneously imposing one or more of the assumptions (A1)–(A7) defined in Section 2 can lead to a *false alarm* (a high PC when the true PC is much lower) or a *misdetection* (a low PC when the true PC is much higher). Figure 3 depicts the false alarm (left) and misdetection (right) cases when the Gaussian assumption at TCA is violated. For the latter, there is no "intersection" between the covariances of the two objects (shown in red and blue) leading to a low PC. However, if the true PDF (of the red object) is non-Gaussian and "bananoid-shaped" as depicted in the figure, then there is a non-trivial intersection between it and the blue covariance ellipsoid leading to a higher PC. Therefore, Gaussian approximations would lead to a misdetection. Figure 3(a) depicts the opposite use case in which Gaussian approximations would lead to a false alarm.

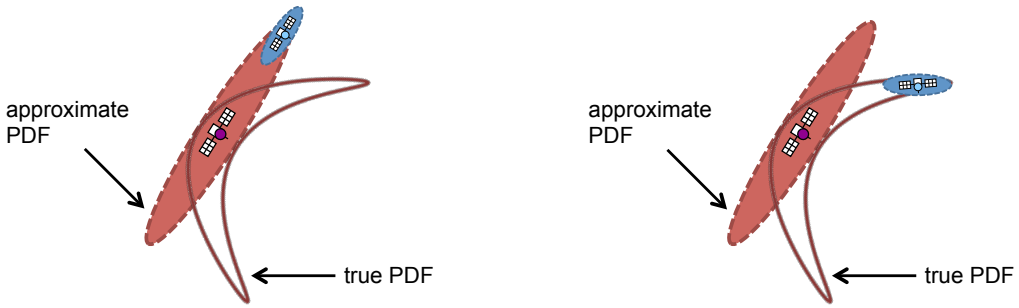

(a) False alarm (b) Misdetection

Figure 3. Impact of Making an Incorrect Gaussian Assumption in PC Analysis

In order to illustrate the value of KRATOS, we developed a simulator that could generate scenarios that demonstrate the false alarm or misdetection cases, using a combination of real and simulated VCMs. In this

section, we present results from processing some of this data showing one false alarm scenario and one misdetection scenario. Table 1 describes some of the details of these scenarios. While for the misdetection case the VCM of the secondary is simulated, the VCM of the primary, namely the ISS, is real. Indeed, one objective of these simulation studies is to show that there exist hypothetical (analyst satellite or UCT) objects that can potentially produce false alarms or misdetections on real satellites such as the ISS. Due to their sensitivity, the precise VCM data cannot be shown in this paper.

Table 1. Description of the False Alarm and Misdetection Scenarios

	False Alarm	Misdetection
Primary Object	80001 (Hypothetical Analyst Sat)	25544 (ISS)
Secondary Object	91002 (Hypothetical UCT)	92002 (Hypothetical UCT)
Conjunction Time	1 day (from epoch)	2.18 days (from epoch)
Screening Interval	2 days	3 days
Combined Radius	75 m	75 m

To cross-validate KRATOS, we implemented a (non-adaptive) version of the AEGIS algorithm [3] that works with the PC algorithm described in DeMars, Cheng, and Jah [2] (see the comment at the end of Section 2). In order to validate the accuracy of the computed PC in KRATOS and AEGIS, we implemented a computationally expensive but highly accurate *Monte-Carlo-based method*. All methods (KRATOS, AEGIS, and Monte-Carlo) were implemented in Fortran, thus permitting runtime comparisons. We remark that the accuracy of the probabilities computed using a Monte-Carlo method can be quantified using the *Chernoff-Hoeffding bound* [13, 14]. Indeed, the number of Monte-Carlo trials N required to achieve a relative accuracy ϵ with a significance level α is given by

$$N > \frac{1}{2(\epsilon P_T)^2} \ln\left(\frac{2}{\alpha}\right), \tag{7}$$

where P_T is the "true" probability. For example, to meet a 1% accuracy ($\epsilon = 0.01$) for a P_T of 0.3 with a 95% confidence level ($\alpha = 0.05$), at least 204,938 independent trials are needed.

Figure 4 shows results from the false alarm scenario. The left panel plots the computed PC versus the number of Gaussian components (used in the secondary object) using the AEGIS and KRATOS methodologies. The 95% confidence region deduced from the Chernoff-Hoeffding bound (7) is displayed in the grey shaded area. The right panel shows the corresponding runtime (on a single thread of a single core) for each configuration. Figure 5 is the analogous figure for the misdetection scenario. Table 2 summarizes the PC and runtime results for these scenarios. In this table, we remark that the PCs quoted for the Gaussian mixture-based approaches (i.e., AEGIS and KRATOS) used 2049 Gaussian components while the Monte-Carlo PCs were computed using 10^9 trials. A number of observations can be made.

Table 2. Summary of Results from the False Alarm and Misdetection Scenarios

Method	PC	Runtime (minutes)
Foster	2.607E-3	∼0
AEGIS	1.664E-5	22.0
KRATOS (EqOE)	2.367E-6	1.40
KRATOS (J_2EqOE)	2.368E-6	1.30
Monte-Carlo	1.932E-5	10,900

(a) False alarm scenario

Method	PC	Runtime (minutes)
Foster	2.065E-14	∼0
AEGIS	1.228E-04	44.0
KRATOS (EqOE)	8.225E-05	1.40
KRATOS (J_2EqOE)	1.226E-04	1.40
Monte-Carlo	1.542E-04	10,800

(b) Misdetection scenario

- In both scenarios, the PCs produced by AEGIS and KRATOS converge as the number of Gaussian mixture components increases. This confirms that the algorithms are performing as expected.
  - In the false alarm scenario, the EqOE and J_2EqOE modes of KRATOS converge to the same value (to within 3 significant figures). AEGIS converges to a different value, however all are within the 95% Chernoff-Hoeffding confidence interval, as deduced from the Monte-Carlo result.

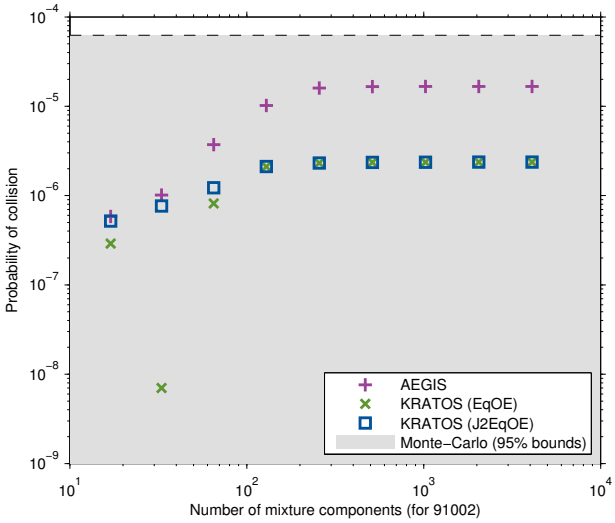

(a) Probability of Collision

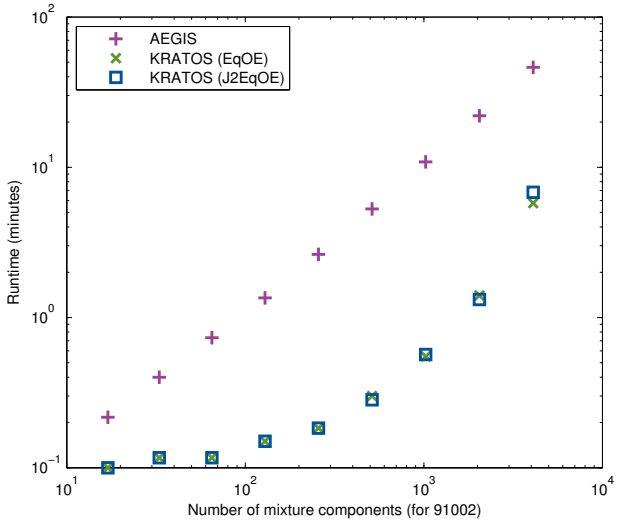

(b) Runtime

Figure 4. False Alarm Scenario Results

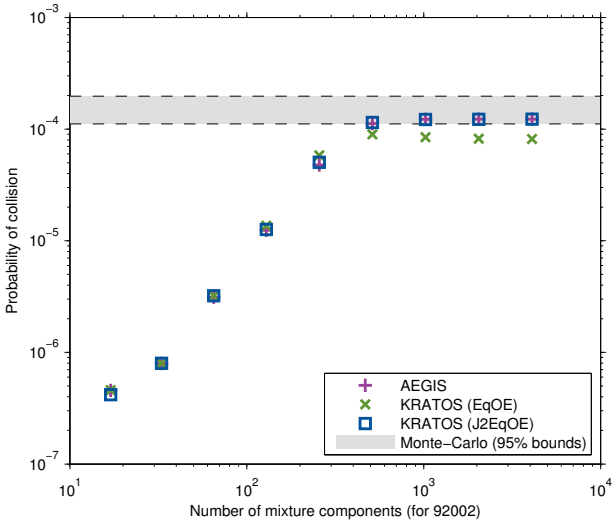

(a) Probability of Collision

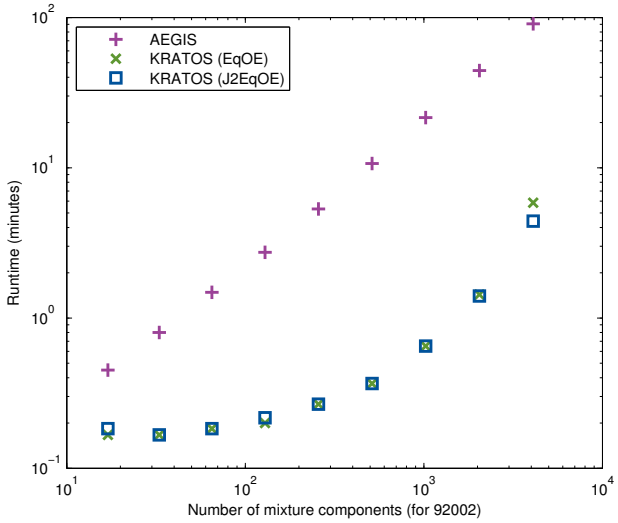

(b) Runtime

Figure 5. Misdetection Scenario Results

  - In the misdetection scenario, KRATOS (J_2EqOE) and AEGIS converge to a common value that agree with the Monte-Carlo result (i.e., they are within the shaded confidence interval). KRATOS (EqOE) converges to a number outside the confidence interval. Although not shown here, the reason for this disagreement is because the uncertainty of the secondary object (i.e., the hypothetical UCT) cannot be represented by a single Gaussian in EqOE coordinates at the nominal TCA. Thus, this example illustrates the value of using the J_2EqOE coordinates over EqOE. The former choice of coordinates to represent uncertainty prolong covariance realism and do not require a significant increase in computational runtime as evidenced in the right panels of Figures 4 and 5.

- In the misdetection scenario, the true PC is nearly 10 orders of magnitude larger than that predicted by the Foster method; the PC is greater than the common 10^{-4} threshold value for which a maneuver would presumably be performed if the spacecraft was operational. As visualized in Figure 6 below, this tail probability is significant. Thus, by using the Foster method, the ISS would likely not maneuver and be at high risk of colliding with the UCT. KRATOS and AEGIS, on the other hand, correctly detect a high-risk

collision event.

- In the false alarm scenario, the true PC is lower than the 10^{-4} threshold. Foster's method, on the other hand, yields a PC over an order of magnitude larger than this threshold and would potentially result in an unnecessary maneuver operation.
- KRATOS is significantly faster than (our implementation of) AEGIS since it only requires propagating a single Gaussian in element space to the nominal TCA.
- KRATOS and AEGIS are orders of magnitude faster than Monte-Carlo simulation and give comparable accuracies.
- KRATOS, AEGIS, and Monte-Carlo techniques are all "embarrassingly parallelizable"; their relative runtimes could be reduced by porting their respective implementations to a high performance computing architecture.

Figure 6 visualizes the misdetection scenario around the TCA. In this picture, the ISS 3-sigma covariance ellipsoid is depicted in blue while the Monte-Carlo particles characterizing the true uncertainty are depicted in purple. The UCT covariance ellipsoid is depicted in red (and has a long thin "sausage shape") while the true particle cloud uncertainty (which resembles a "banana shape") is depicted in orange. We see that the ISS covariance ellipsoid comes nowhere near the UCT covariance ellipsoid resulting in the infinitesimally small PC produced by the Foster method and hence the misdetection. On the other hand, we see that many of the UCT particles (in orange) penetrate the ISS covariance ellipsoid (in blue) that lead to a non-negligible PC that would warrant evasive action. KRATOS is able to accurately model the true uncertainties of the objects (i.e., the particle clouds) by way of Gaussian mixtures leading to the correct PC being computed.

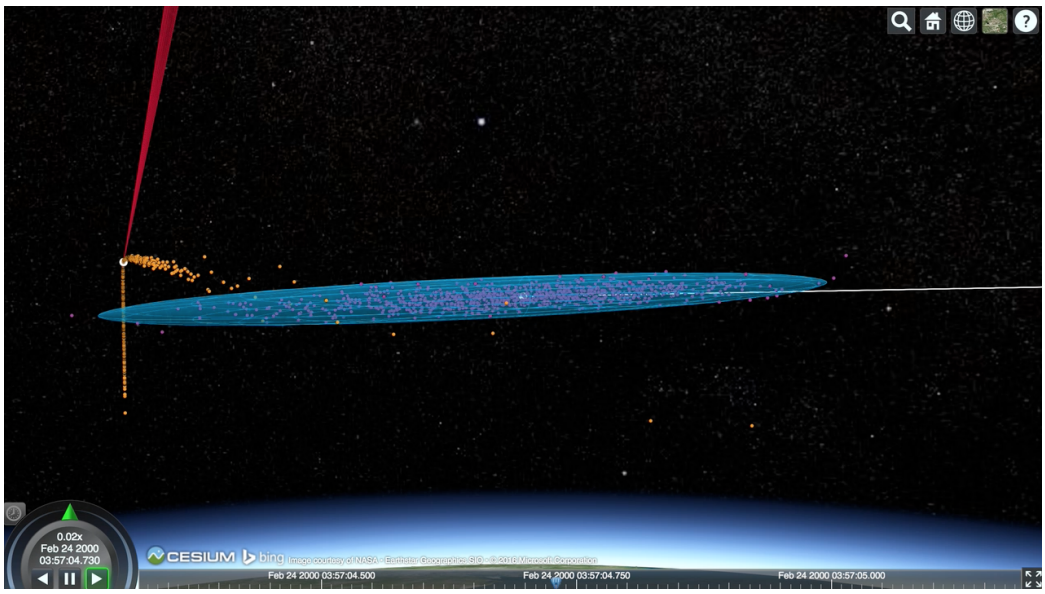

Figure 6. Visualization of the Misdetection Scenario

4. PATH FORWARD

Table 3 puts things into perspective by reviewing the main assumptions imposed in KRATOS, other PC methodologies, and the new KRATOS v2 presently under development. Two main enhancements are underway for KRATOS v2:

Table 3. Assumptions Imposed in KRATOS and Other PC Methodologies

	PC Methodology				
Assumption	Foster	AEGIS	KRATOS	KRATOS v2	Monte-Carlo
Short encounter time	■	■	■	□	□
No velocity uncertainty	■	■	■	□	□
Constant positional covariance	■	□	□	□	□
Gaussian distribution	■	□	□	□	□

1. Use of a more robust PC algorithm that treats medium and long-term encounters (in addition to the short duration encounters already being addressed) and more challenging regimes containing velocity uncertainty by automatically choosing the correct formulation of the PC integral based on what assumptions in Table 3 are met.

2. Improved automation by adaptively selecting the number of Gaussians needed to faithfully represent the PDFs of the primary and secondary RSOs around the nominal TCA (presently, these numbers are input parameters).

While the results presented in Section 3 demonstrate the existence of misdetection and false alarms produced by the Foster method using a combination of real and simulated data, simulation studies will need to be performed to quantify misdetection and false alarm rates for the different PC tools using larger datasets of real historical VCMs of catalogued RSOs and analyst satellites. This will allow us to assess the utility of KRATOS.

Finally, we remark that all of the merits of KRATOS are for naught if the input is invalid. For example, if sensors misreport their measurement errors, then any tracks, orbits, or VCMs produced by processing sensor observations in an orbit determination procedure (e.g., batch differential correction) will have dubious state and covariance information. What is more, sensor measurements are usually provided in "B3-format," which have limited precision and, for the case of radars, are filtered or correlated. The latter is particularly unsettling given that traditional orbit determination and Kalman filtering methods implicitly assume that all input measurements are uncorrelated (independent). As demonstrated by Alfriend *et al.* [15], such covariances are often overly optimistic (too small); small changes in the covariance can create much larger changes in the PC. To address these sensor-level issues, Numerica is presently developing a tool to provide higher quality sensor tracks with more realistic states and covariances, as well as addressing the limitations of B3 data, in order to improve reliability of downstream SSA functions such as UCT resolution and CA.

5. CONCLUSIONS

KRATOS provides a novel approach to computing the PC between RSOs that supports the mission's goal of performing CA screening further out into the future. Some of the key innovations in KRATOS include (i) thinking beyond "Gaussianity" by treating bananoid-shaped uncertainties and other non-Gaussian distributions in an effort to reduce misdetections and false alarms; (ii) using Gaussian mixture representations to achieve a high level of computational efficiency; and (iii) representing RSO uncertainty in the J_2 equinoctial orbital elements to significantly prolong covariance realism. It was demonstrated that a traditional technique (i.e., Foster's method) can produce misdetections and false alarms. KRATOS informs the correct courses of action at a substantially reduced computational cost compared to that of Monte-Carlo simulation, especially in low PC scenarios around the threshold at which the decision to maneuver would be made, and when a large number of Monte-Carlo trials would be needed. Ongoing work will further mature KRATOS and demonstrate its utility on large (real) datasets.

ACKNOWLEDGMENTS

The authors thank Terry Alfriend and Alex Ferris for fruitful technical interactions. This work was funded, in part, by a Phase I SBIR from the Air Force Research Laboratory Space Vehicles Directorate (FA9453-15-M-0482) and a Phase II SBIR from the Air Force Research Laboratory Aerospace Systems Directorate (FA8650-16-C-9204).

DISTRIBUTION

Approved for public release (Case Number OPS-16-12457).

REFERENCES

1. J. Foster, "A parametric analysis of orbital debris collision probability and maneuver rate for space vehicles," Tech. Rep. JSC-25898, NASA, 1992.
2. K. J. DeMars, Y. Cheng, and M. K. Jah, "Collision probability with Gaussian mixture orbit uncertainty," *Journal of Guidance, Control, and Dynamics*, vol. 37, no. 3, pp. 979–985, 2014.
3. K. J. DeMars, M. K. Jah, Y. Cheng, and R. H. Bishop, "Methods for splitting Gaussian distributions and applications within the AEGIS filter," in *Proceedings of the 22nd AAS/AIAA Space Flight Mechanics Meeting*, (Charleston, SC), February 2012. Paper AAS-12-261.
4. J. M. Aristoff, J. T. Horwood, and K. T. Alfriend, "On a set of J_2 equinoctial orbital elements." (Submitted to AFRL/RV for public release approval), 2016.
5. S. Alfano, "Review of conjunction probability methods for short-term encounters," in *Proceedings of the 17th AAS/AIAA Space Flight Mechanics Meeting*, (Sedona, AZ), January 2007. Paper AAS-07-148.
6. J. T. Horwood, N. D. Aragon, and A. B. Poore, "Gaussian sum filters for space surveillance: theory and simulations," *Journal of Guidance, Control, and Dynamics*, vol. 34, no. 6, pp. 1839–1851, 2011.
7. J. T. Horwood, J. M. Aristoff, N. Singh, and A. B. Poore, "A comparative study of new non-linear uncertainty propagation methods for space surveillance," in *SPIE Proceedings: Signal and Data Processing of Small Targets 2014*, vol. 9092, 2014.
8. S. J. Julier, J. K. Uhlmann, and H. F. Durant-Whyte, "A new method for the nonlinear transformation of means and covariances in filters and estimators," *IEEE Transactions on Automatic Control*, vol. 55, pp. 477–482, 2000.
9. J. T. Horwood and A. B. Poore, "Adaptive Gaussian sum filters for space surveillance," *IEEE Transactions on Automatic Control*, vol. 56, no. 8, pp. 1777–1790, 2011.
10. J. M. Aristoff, J. T. Horwood, N. Singh, and A. B. Poore, "Nonlinear uncertainty propagation in orbital elements and transformation to Cartesian space without loss of realism," in *Proceedings of the 2014 AAS/AIAA Astrodynamics Specialist Conference*, (San Diego, CA), August 2014. Paper AIAA-2014-4167.
11. A. B. Poore, J. M. Aristoff, and J. T. Horwood, "Covariance and uncertainty realism in space surveillance," Tech. Rep. Astrodynamics Innovations Committee (AIC) Covariance Realism Working Group, September 2016. (To Appear).
12. V. T. Coppola, "Including velocity uncertainty in the probability of collision between space objects," in *Proceedings of the 22nd AAS/AIAA Space Flight Mechanics Meeting*, (Charleston, SC), January 2012. Paper AAS-12-247.
13. H. Chernoff, "A measure of asymptotic efficiency for tests of a hypothesis based on the sum of observations," *Annals of Mathematical Statistics*, vol. 23, pp. 493–507, 1952.
14. W. Hoeffding, "Probability inequalities for sums of bounded random variables," *Journal of the American Statistical Association*, vol. 58, no. 301, pp. 13–30, 1963.
15. K. T. Alfriend, M. R. Akella, J. Frisbee, J. L. Foster, D. J. Lee, and M. Wilkins, "Probability of collision error analysis," *Space Debris*, vol. 1, pp. 21–35, 1999.